JOURNAL OF MATERIALS SCIENCE 26 (1991) 5671–5680

Accelerated fatigue fracture mechanism of medium density polyethylene pipe material

J. J. STREBEL, A. MOET
Department of Macromolecular Science, Case Western Reserve University, Cleveland, OH 44106, USA

Fatigue crack propagation studies were performed in medium density polyethylene pipe to elucidate the damage mechanism associated with pipe failure. Past pipe testing methods required up to several years to produce failures which mimicked those observed in the field. However, by fatiguing a specially designed test specimen, brittle failure, resembling that observed under service conditions, was produced in only three days. It was determined that the method of loading and the crack plane orientation greatly affect the degree and extent of brittle crack propagation. In some specimen geometries, the initial brittle fracture may undergo a transition to a more ductile failure mode. The damage which precedes the crack tip during brittle cracking is a root craze and two smaller side crazes; these crazes are primarily composed of yielded membranes which are oriented normal to the crack propagation direction, rather than being composed of fibrils. The number and length of these crazes was shown to be dependent on the chosen test geometry.

1. Introduction

Long-term load-bearing structural components, such as polyethylene fuel gas pipes, require accelerated testing to ascertain satisfactory service life performance. Many accelerated pipe test methods have been developed. Some of these methods are: the hydrostatic strength test [1], constant tensile load method [2], compressed ring test [3], and bent strip test [4]. Elevated temperatures and/or environmental stress cracking agents have also been used with these tests to accelerate failure [5, 6]. Regardless of the test method chosen, it should be capable of producing quickly a brittle crack that mimics cracks observed in the field, and it should be based on a sound theoretical foundation.

As most of the above-mentioned methods require formidably long times (up to several years) to produce brittle failures, fatigue has been used to accelerate brittle cracking [7–9]. Fatigue significantly reduces the testing time and can be used to mimic field failure. Fundamental material parameters can also be extracted from fatigue tests by applying thermodynamics to the irreversible cracking process [8]. Therefore, fatigue methods meet all the requirements of an accelerated pipe test.

In this paper, we will focus on one aspect of fatigue testing – the mechanism of crack propagation. Through careful sectioning and microscopy, we will determine the fatigue mechanism and show how different loading methods and crack plane orientations can be used to re-create field failure in the laboratory. We will also examine the microstructure of the craze which precedes the crack and see how it differs from crazes observed in other polymers.

2. Experimental procedure

Extruded medium-density ethylene/butene copolymer (MDPE) pipe, which was produced in the 1960s, was provided by Philadelphia Electric Co. The pipe had an average outside diameter of 115 mm and a minimum wall thickness of 11 mm. Several different specimen geometries were prepared from the pipe (Fig. 1). These geometries are designed to examine the effect of specimen thickness, plane of crack propagation and loading configuration on the fracture mechanism (Table I).

One of these geometries was a 28 mm wide arc-shape specimen with stainless steel reinforced 6 mm diameter loading holes drilled 25 mm apart. A 2.5 mm deep razor notch was introduced equidistant from each loading hole on the inner radius of the arc after the specimen had been placed in liquid nitrogen for approximately 30 min to reduce notch tip damage. After the specimen was secured in an MTS servo-hydraulic testing machine with a pair of clevis grips (Fig. 2), it was subject to sinusoidal tension–tension fatigue at 0.5 Hz, using a maximum load of 5.62 MPa ($\sim 25\%\ \sigma_y$). An R ratio ($\sigma_{min}/\sigma_{max}$) of 0.1 was used to minimize creep effects.

The other specimens – single edge notch, block, and trapezoid – were milled from the locations shown in the pipe in Fig. 1. These specimens were notched to a 2.5 mm notch depth on the side which was closest to the inner radius of the pipe. They were then secured with regular flat grips and subject to the same loading conditions as the arc specimen.

In order to determine the evolution of damage associated with the crack tip, some arc tests were interrupted and the specimens were removed prior to failure. Sections to observe the damage zone sur-

0022–2461/91 $03.00 + .12

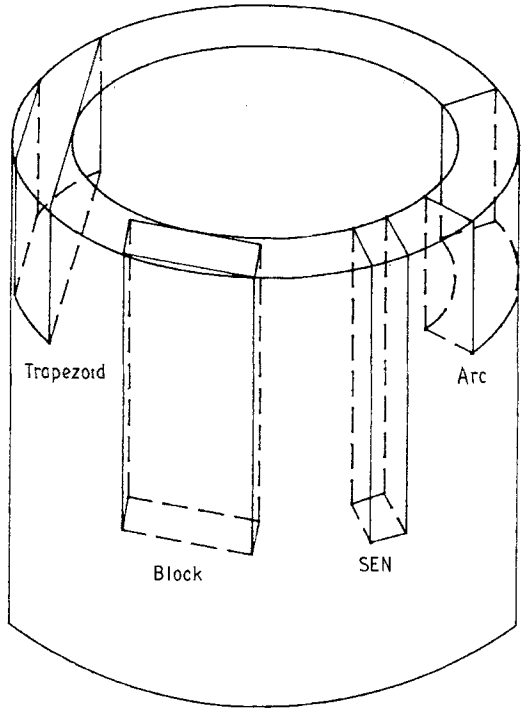

Figure 1 Origin of specimen geometries in the pipe.

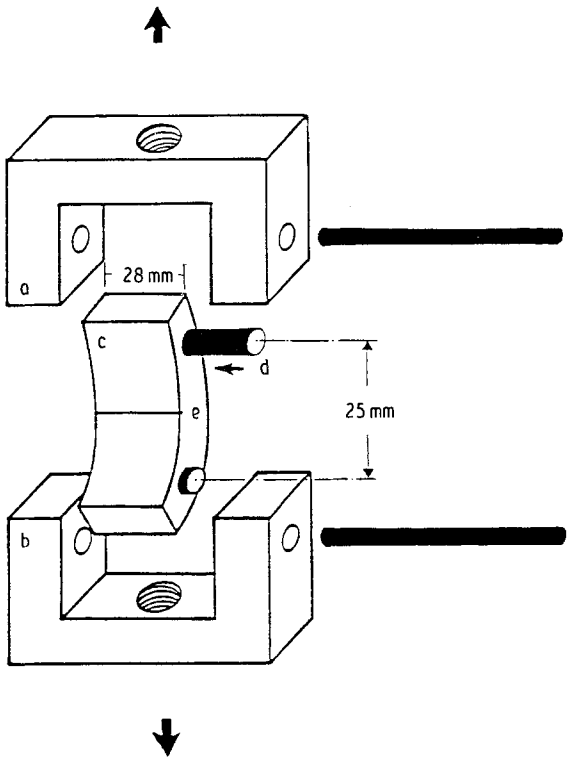

Figure 2 Schematic diagram of arc specimen and its gripping fixtures: (a) and (b) upper and lower clevis grips, (c) arc specimen, (d) reinforcing steel tube, and (e) notch. The vertical arrows represent the loading direction.

rounding the crack were prepared by using a low-speed saw to cut the specimens in a plane parallel to the crack propagation direction and orthogonal to the fracture surface (side view). Sections in a plane parallel to the crack front and orthogonal to the fracture surface were also removed from the damage zone (front view). Because of the high degree of pigmentation in the pipe material, it was necessary to thin each section to 100 μm and to apply a permanganate–acid etchant to elucidate the damage zone [10]. After completing this procedure, transmitted light microscopy was used to determine the size and evolution of the craze zone.

Some samples were stretched to their original displacement and then gold-sputtered so that the craze microstructure could be observed on a Jeol JSM 35CF scanning electron microscope.

TABLE I Specimen configurations

Specimen	Dominant stress state	Loading method	Crack plane orientation
Arc	Plane strain	Point load (pins)	C–R
SEN	Plane stress	Uniform far field	L–R
Block	Plane strain	Uniform far field	L–R
Trapezoid	Plane strain	Distributed point load (gripped near fracture)	C–R

3. Results and discussion

As discussed earlier, most pipe test methods require formidably long test times to produce a fracture which resembles the brittle failures which are generally associated with gas pipeline leaks. This testing time can be reduced by increasing the load. However, the resulting failure then becomes ductile. Thus, a great need has existed for a pipe test method which *quickly* produces a failure that mimics failures observed in the field. By using fatigue as an accelerating agent, we have designed a test which produces a fracture surface which is nearly identical to that of a field failed pipe. To develop such a test, the mechanism of crack propagation was scrutinized in the arc specimen, and then the effects of the loading method and crack plane orientation on the failure mode were determined. Therefore, the following section will describe in detail the fracture mechanism observed in the arc specimen. The arc specimen was extensively studied because of its greatly reduced testing time as compared with the other test geometries (Table II). This shorter testing time permitted the fracture and interrupted fracture of more specimens, and hence a better understanding of the failure mechanism. The last section will then show that while the same fracture mechanism exists in all of the test geometries, certain factors (loading method and crack plane orientation) affect the extent of damage, and hence the brittleness of the fracture. By correctly setting these variables, a pipe test has been designed that re-creates field failure in less than three days.

3.1. Mechanism of crack propagation

3.1.1. Brittle–ductile failure regions

The first indication of the crack propagation mechanism may be obtained from the fracture surface of the arc specimen. A low-magnification micrograph shows evidence of two different regions (Fig. 3). During the early stages of crack propagation, the fracture surface is macroscopically flat with four apparent arrest lines,

TABLE II Kinetics of crack propagation for different specimen configurations

Stage	Number of cycles			
	Arc	Block	Trapezoid	SEN
Crack initiation	11 000	22 000	90 000	44 000
Brittle crack propagation	9000	37 000	29 000	87 000
Ductile crack propagation	10 000	1000	1000	4000
Total	30 000	60 000	120 000	135 000

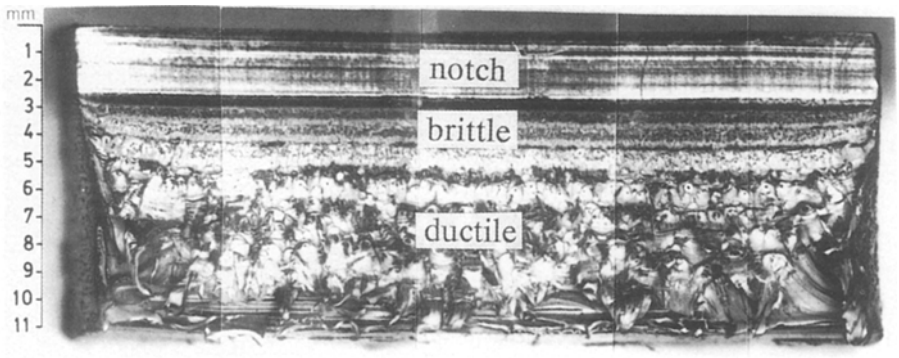

Figure 3 Fracture surface of arc specimen showing the notch and the brittle and ductile crack propagation regions.

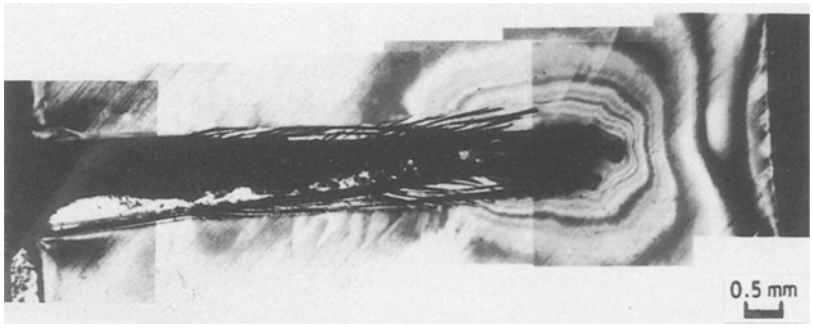

Figure 4 Birefringent zone of arc specimen indicating large-scale yielding and/or orientation in the ductile crack propagation region.

indicative of a discontinuous brittle failure. As the crack length increases, the fracture surface becomes rougher due to the presence of more yielded material. In this ductile region, if there are any arrest bands, they are hidden by the large retracted fibrils. This transition in fracture surface topography is indicative of a change in the fracture mechanism from a brittle failure mode to a ductile one.

This gradual brittle to ductile transition can also be observed by removing a thin section from a plane normal to the fracture surface and parallel to the crack propagation direction (side view). Upon examination of this section under cross-polarized light, one immediately notes a large birefringent zone, which is indicative of significant material yielding and orientation (Fig. 4). This zone indicates the extent and location of ductility during crack propagation. At shorter crack lengths, the size of the zone is very small, reflecting the constrained ductility in that area. However, near a 5 mm crack length the birefringent zone becomes much larger, which is an indication of the increasing amount of ductility associated with the fracture. The point of birefringent zone expansion is concurrent with the change in fracture surface topography and the development of extensive side crazing. All these features demonstrate that the initial brittle fracture becomes progressively more ductile as the crack grows.

Fig. 4 also shows that, within the brittle crack propagation region, a number of crazes are associated with the crack. As the crack propagates, the number and size of crazes increases and the large-scale material yielding, as evinced by the birefringent zone, is superimposed on these crazes. Since damage during brittle crack propagation is composed of crazes, and since very brittle cracks (like those in field-failed pipe) have very small damage zones, we must first understand the crack propagation mechanism and then reduce the extent of crazing associated with brittle crack propagation in order to mimic field failure.

3.1.2. Discontinuous crack growth

Having identified the brittle and ductile regions of crack propagation, a closer examination of the brittle region of the arc specimen's fracture surface is warranted. Low-magnification scanning electron microscopy shows that each arrest line and the corresponding propagation band display a similar structure to the previous arrest line and band (Fig. 5). By looking across a propagation band in the crack propagation direction, it is noted that the macroscopically flat propagation band has an intial area which is microscopically rough. The surface of the band becomes progressively smoother as the next arrest line is approached. This change in fracture surface features is repeated in each band. The only apparent difference between bands is the increased band width and larger broken fibrils at longer crack lengths. The following discussion will demonstrate that these repeating discontinuities are a result of the evolving craze zone which precedes the crack.

Higher magnification of a propagation band reveals a great deal of material deformation, voiding, and micro-scale yielding (Fig. 6). From this observation, it is clear that the macroscopically flat brittle failure regime involves constrained local ductility. The ductility becomes less constrained as the crack length increases, and the amount of material yielding increases as a consequence.

From the similar arrest lines and yielded material, the fracture surface shows that some type of repetitive, discontinuous mechanism – which becomes more ductile at longer crack lengths – controls fracture in this specimen. However, it would be difficult to deduce a model of crack propagation from the fracture surface alone. Therefore, by also examining the micrographs of interrupted arc experiments, the mechanism of crack propagation can be better defined.

3.1.3. Damage-zone profiles

Cracks were propagated to a preset length, at which the arc specimens were removed from the machine,

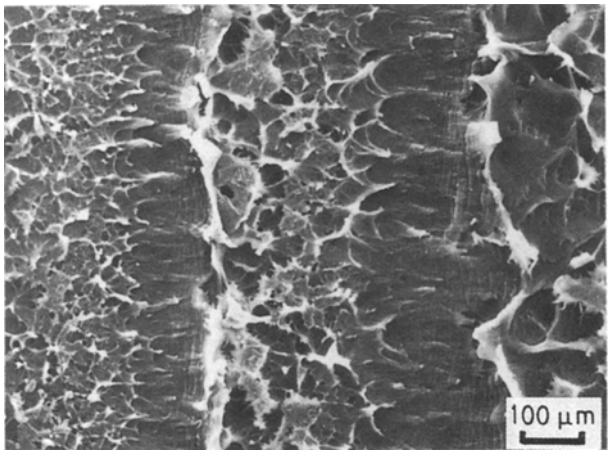

Figure 5 Low-magnification SEM micrograph of brittle crack propagation region of fracture surface. The vertical arrows mark the position of the arrest lines. The crack propagation direction is from left to right.

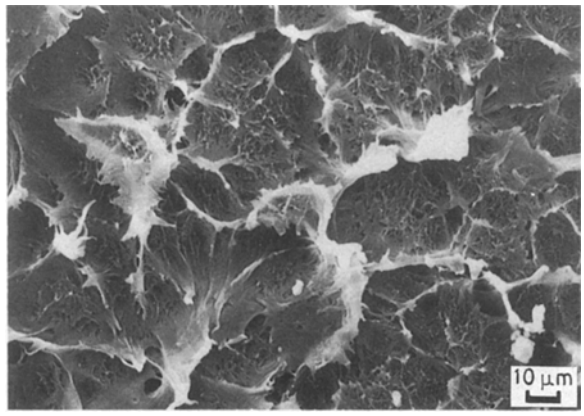

Figure 6 Higher-magnification SEM micrograph of brittle crack propagation region of fracture surface showing microductility.

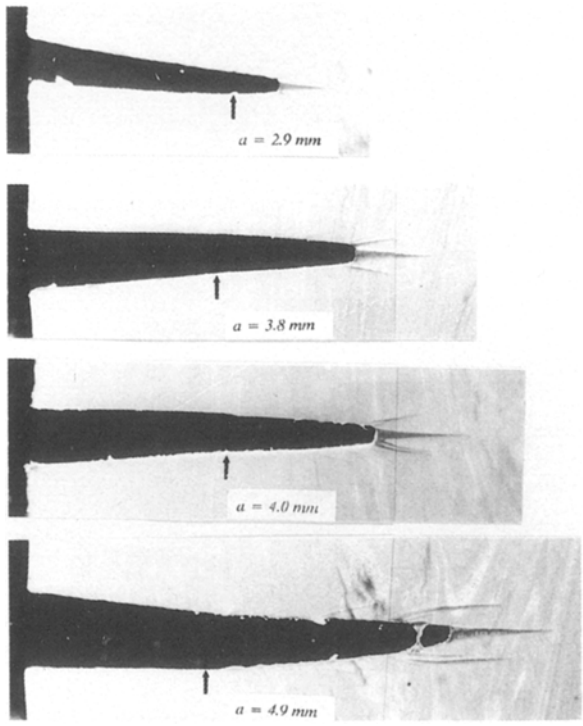

Figure 7 Sections removed from the centre of interrupted arc specimens. The craze zone maintains the same configuration but increases in size with crack length.

and a thin section normal to the crack plane and parallel to the crack propagation direction was removed from the center of the specimen. The damage in these "side views" is representative of what is happening throughout the majority of the specimen; the plane stress effect of the edge masks the interior craze zone. At each crack length, the side views of the damage zone show a large wedge-shaped main craze – the root craze – which extends into the material from the crack tip (Fig. 7). Side crazes, which usually originate at or near the crack tip, are observed above and below the root craze. Polyethylene craze zones of similar shape have been previously reported under different loading conditions [11–13]. Damage zones, consisting of main root crazes and smaller "peripheral" crazes, similar to our side crazes, have also been reported in fatigued polypropylene [14].

The flanking structures of the damage zone have been termed "side crazes" because their microstructure is similar to the root craze; however, it should be realized that a shear component exists with these side crazes. A shear displacement across the side crazes is indicated by the misalignment of extrusion lines through which the side crazes have propagated (Fig. 8). Swei *et al.* [11] observed a similar damage zone in monotonically loaded polyethylene, and by using birefringence, they concluded that the flanking structures resembled shear bands. It has also been noted that under certain loading conditions in polystyrene, crazes and shear bands may have a very similar morphology [15]. Thus, our side crazes display some characteristics of both shear bands and crazes.

These side crazes and the much larger main root craze constitute the damage zone which precedes the crack. This craze zone maintains the same configuration while in the brittle regime, but grows in overall size as the crack length increases. Upon entering the ductile regime (crack length > 5 mm), the length and number of side crazes increases and the spacing of the side crazes becomes irregular (Figs 4 and 8). The sequence of micrographs from the brittle crack propagation regime shows that as the crack advances, it grows through the root craze, leaving the side crazes to collapse along the free surface of the newly formed crack (Fig. 7). The crack will arrest as it approaches the end of the root craze because of a lack of sufficient damaged material through which it may propagate. From the arrested crack tip a new set of root and side crazes will develop, and the cycle will be repeated.

This model of damage growth and brittle crack propagation is supported by comparing the fracture surface and a side view of a failed specimen. It is generally agreed that the lines on the fracture surface which are orthogonal to the crack propagation direction are the result of an arrested crack front, and hence are referred to as arrest lines. Since these arrest lines would mark the position of a temporarily stationary crack tip, according to the proposed propagation mechanism, a side craze should occur under, and originate at, each arrest line. Fig. 9 is a montage of the fracture surface and corresponding side view of a failed arc specimen. (The thin vertical lines are caused by the overlaying of micrographs and not a result of the fracture process.) This figure indeed shows that each arrest line on the fracture surface marks the origin of a side craze below the fracture surface. Therefore, it appears that the proposed discontinuous crack propagation mechanism is quite accurate. A similar fatigue crack propagation mechanism and an analogous damage zone have been identified in polycarbonate [16]. Skibo *et al.* [17] have also identified the same type of discontinuous crack propagation mechanism in several different polymers.

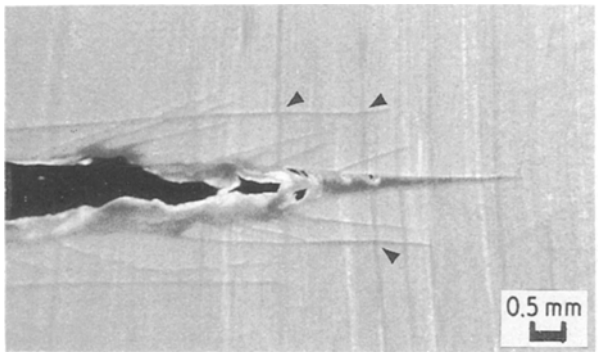

Figure 8 Micrograph of the crack tip and surrounding damage in the ductile crack propagation region ($a = 6.9$ mm). The arrows mark shear displacement in extrusion lines which have been intersected by side crazes.

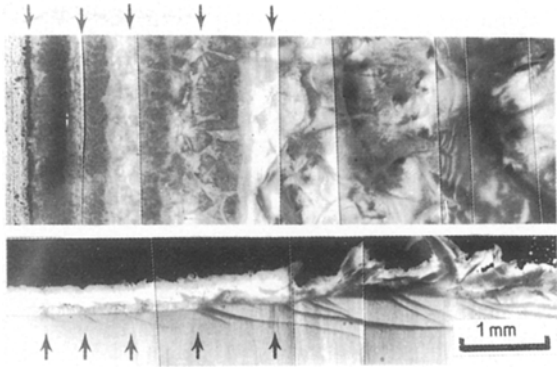

Figure 9 Montages of the partial fracture surface and corresponding side view of an arc specimen, showing the correlation between the arrest lines and the origin of side crazes. (The thin vertical lines are a result of overlaying the micrographs and not a result of the fracture process).

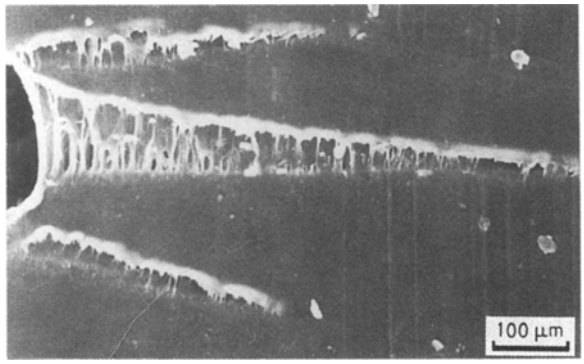

Figure 10 SEM micrograph of voids and continuous material yielding in the root craze.

3.1.4. Craze microstructure

As crazes constitute the damage mechanism associated with brittle failure, and since the purpose of this study was to understand brittle failure in polyethylene pipe material, a closer look at the craze microstructure is in order. A section such as the one in Fig. 4 was removed from the centre of the specimen while the crack was still within the brittle crack propagation region and was examined using SEM. The damage in this section is representative of the damage through most of the specimen thickness; plane stress yielding is present near the edges. This section (Fig. 10) shows

that the damage mechanism within the root craze is a combination of fibrillation and continuous material yielding. Continuous material yielding represents the dominant mode of deformation at the craze tip, but the larger craze opening displacement near the crack tip favours deformation by fibrillation. However, these fibrils are not well-defined single entities like those in the image of a polystyrene craze [18]. Rather, the "fibrils" appear to be the ends of fibrillated membranes which extend through the craze in a direction which is relatively parallel to the crack front (Fig. 11). A very similar yielded film has been observed at the crack tip in creeped polyethylene. The existence of the film was attributed to a localized plane stress state within the thick specimen [13]. These membranes are not singular, but rather, are interconnected to form a network of yielded material. This continuous yielded material is comparable to the fibrous sheets observed in tensile fractured shear bands [19]. The similarity of these structures again suggests shear deformation within the craze zone. The voids which occupy the space between the membranes in the arc specimen may be considered as capped tunnels which vary in size and shape and may be connected by tears or holes in the membrane. The existence of varying degrees of these features throughout the craze results in an extremely complex craze microstructure.

If sections which are orthogonal to the sections above are removed from the damage zone, a more comprehensive vision of the craze zone can be attained. Such a front view, observed at the crack tip, in which the crack propagation direction is into the page, shows the presence of the continuous membrane which was discussed above (Fig. 12). Although the membrane appears impervious, at higher magnification, fibrillation and the accompanying voids may be observed (Fig. 13). On the other hand, there are also flat regions of continuously yielded material which may appear relatively close to the fibrillated region. The fibrillation of the membrane is a result of the high degree of strain across the craze. The material contracts laterally as the membrane is strained (Poisson effect), thus resulting in voids. The fibrillar size varies from about 130 to 230 nm, which is much larger than the 4 to 60 nm fibril diameter observed in many glassy polymers [20]. However, we have estimated the volume of material within the craze to be about 50%, which lies in the 40–60% range observed for other plastics [20]. Upon fracture, it is the broken fibrils which were originally part of the membrane network that are observed on the fracture surface.

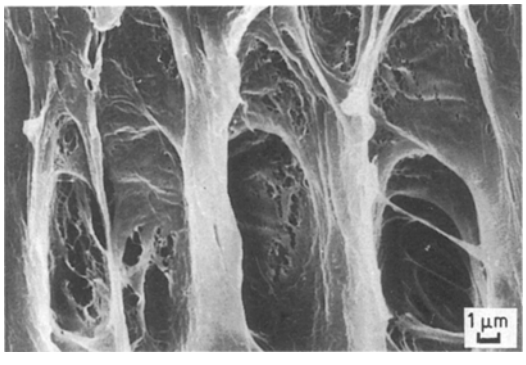

Figure 11 SEM micrograph of membrane ends in the root craze. The crack propagation direction is from left to right.

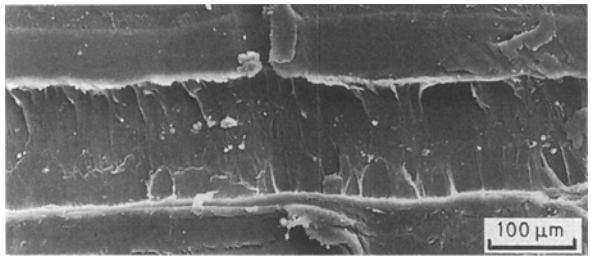

Figure 12 Continuous yielded membrane found in the root craze. Crack propagation direction is into the page.

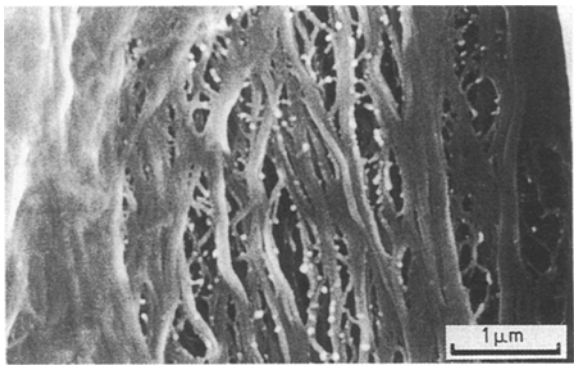

Figure 13 Fibrillation of membrane in Fig. 12.

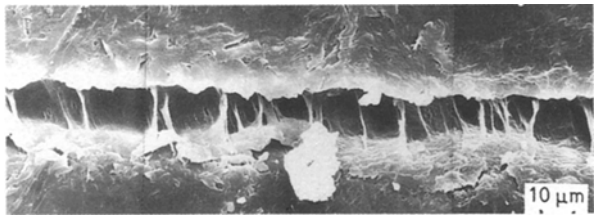

Figure 14 Craze morphology near the craze tip is a combination of voiding and membrane yielding. Crack propagation direction is into the page.

Another section which was removed in the same plane but closer to the craze tip (Fig. 14) revealed a structure which closely resembled the structure observed in the side views. This other front view shows areas of continuous yielded membranes and columns of vertically oriented material, which are the ends of other membranes oriented in the crack propagation direction. Thus, it can be concluded that at the crack tip, a large yielded membrane is oriented along the crack front, and the supporting structure within the craze is a network of randomly oriented membranes.

3.2. Increasing the brittle failure contribution

3.2.1. Effect of specimen thickness on crack propagation mechanism

Having established the crack propagation mechanism and craze microstructure, the effect of several variables

on the extent of brittle crack propagation will be investigated. Specifically, we would like to be able to examine the effect of crack – specimen configuration on the magnitude of the brittle crack propagation region. The first variable to be examined which may affect the brittleness of failure is the effect of the specimen thickness. In order to do this, a 2 mm thick single edge notch (SEN) and a much thicker (28 mm) block specimen are compared under the same loading conditions (Fig. 1 and Table I).

Fig. 15 shows montages of the complete fracture surface of the SEN and a partial fracture surface of the block specimen. These micrographs show that while the block specimen has a relatively flat fracture surface throughout its width, the SEN specimen demonstrates material yielding and pull-out in the later stages of crack propagation. Since a flat fracture surface is an attribute of brittle failure, this difference indicates that the block specimen produces a more brittle failure than does the SEN. If one examines the corresponding side views of these specimens (Fig. 16), the same conclusion can be drawn. Where the block specimen has small thin singular side crazes, the SEN has thick groups of side crazes. These micrographs show that the extent of crazing was greater during crack propagation in the SEN specimen; hence, because of the smaller amount of crazing and flatter fracture surface, the block specimen produced a more brittle failure than the SEN. The same mechanism exists in both these specimens. However, the plane strain condition has constrained the amount of crack tip damage (crazing).

3.2.2. Effect of crack plane orientation and specimen bending

Although it is not surprising that the thicker (more plane-strain contribution) block specimen produced a more brittle failure than the SEN specimen, it is surprising that the arc, which is the same thickness (28 mm) as the block, produces a shorter brittle crack propagation region than does the SEN (Fig. 17). If the

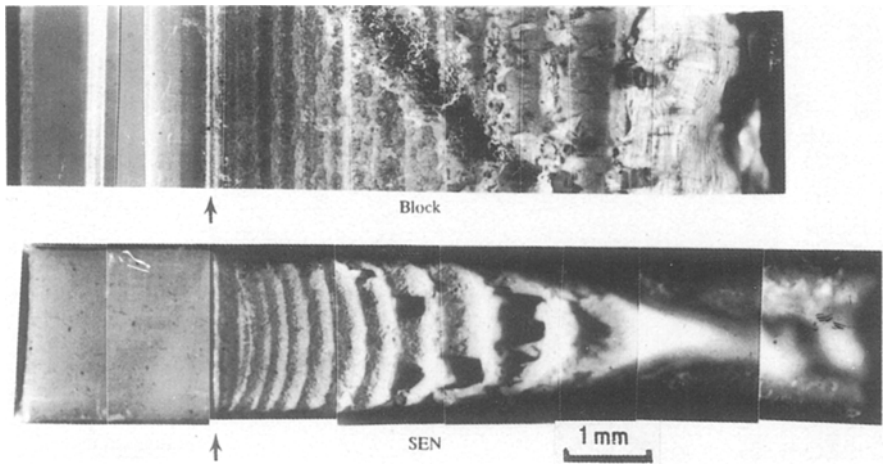

Figure 15 Montages of the complete SEN fracture surface and partial block fracture surface. The vertical arrows mark the notch position.

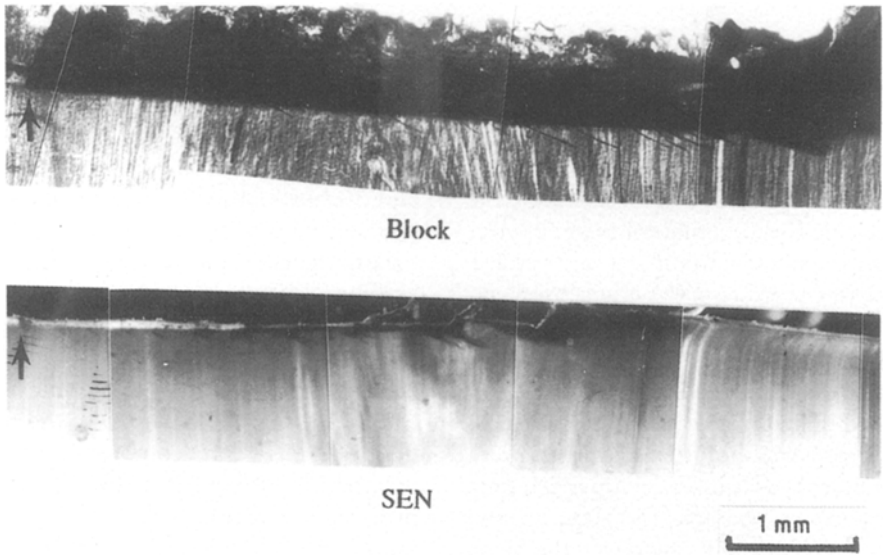

Figure 16 Montages of side views of SEN and block specimens. The vertical arrows mark the notch position.

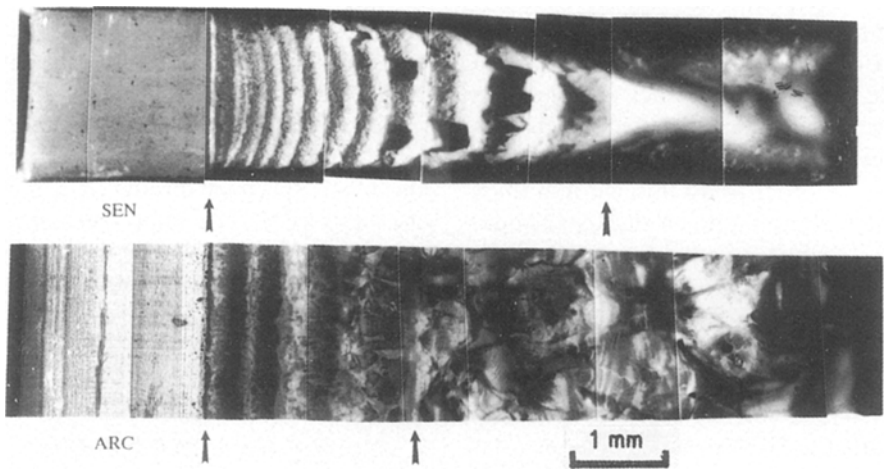

Figure 17 Montage of the complete SEN fracture surface and partial arc fracture surface. The vertical arrows mark the notch position and the beginning of complete ductile failure. The crack propagation direction is from left to right.

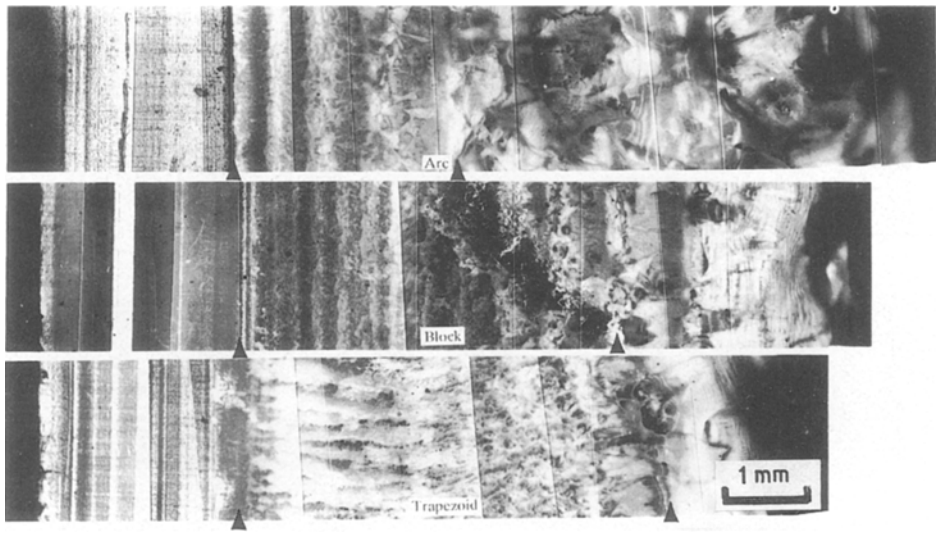

Figure 18 Montages of the partial fracture surfaces of the arc, block, and trapezoid specimens. The vertical arrows mark the notch position and the beginning of complete ductile failure. The crack propagation direction is from left to right.

origins of the block and arc specimens are compared (Fig. 1), two differences are immediately noticed. The first difference is that the crack plane orientations are different in these two specimens (Table I). The block has an L–R and the arc has a C–R crack plane orientation [21]. Using this designation the first letter represents the direction normal to the fracture surface, while the second letter represents the crack propagation direction: L = longitudinal, R = radial, C = circumferential. The other difference is the load distribution associated with each specimen. Whereas the block specimen had a uniformly distributed far-field load, the arc specimen was point-loaded (pins went through the specimen). Because of this gripping method, the arc specimen was free to rotate around the pins as the crack propagated; obviously, the block specimen could not rotate. The trapezoid specimen was created because of these two differences (Fig. 1). This specimen is very similar to the arc. However, it was created with two parallel faces so that it could be loaded using standard flat grips which prevent specimen rotation. Therefore, by comparing the trapezoid and the block, the effect of crack plane orientation can be determined, and by comparing the trapezoid and the arc the effect of the arc specimen's rotation on the loading pins can be determined.

Fig. 18 is a comparison of montages of the partial fracture surfaces of the arc, block, and trapezoid specimens. (The frequent vertical lines are a result of the overlaying of micrographs and not a result of the fracture process.) By comparing the trapezoid and the arc fracture surfaces, it is obvious that the brittle crack propagation region is much larger in the trapezoid than it is in the arc. This difference indicates that specimen rotation must be subdued to increase the extent of brittle crack propagation. From Fig. 18 it

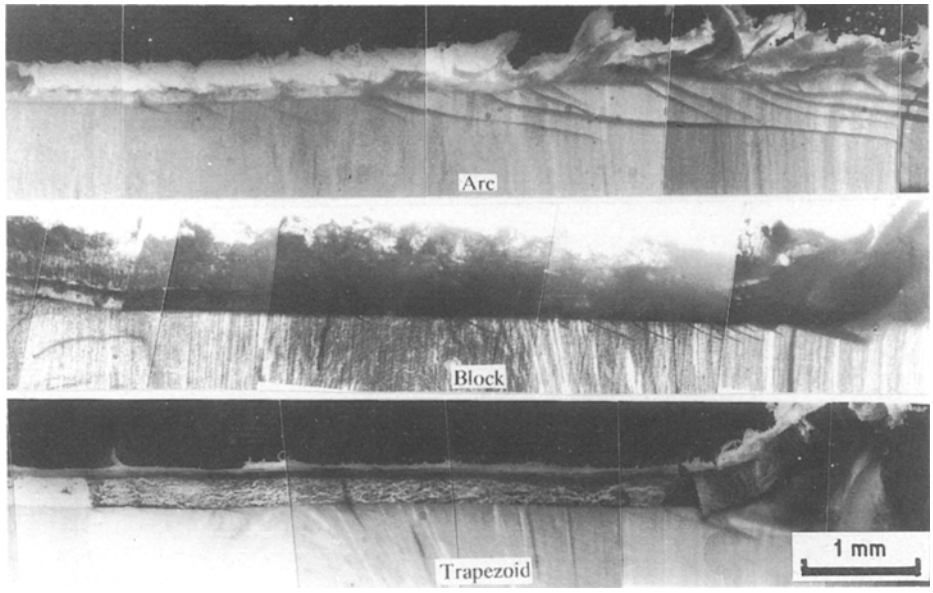

Figure 19 Side views of arc, block, and trapezoid specimens.

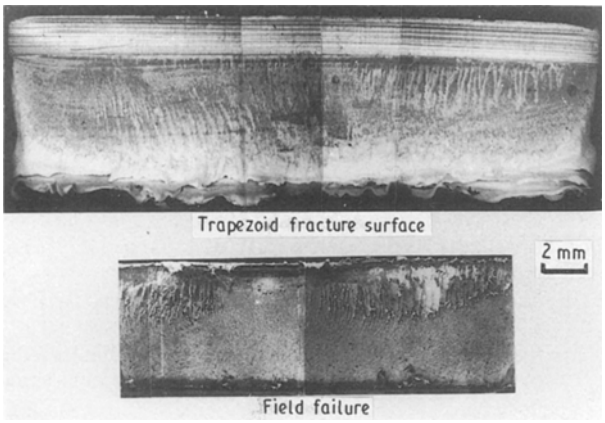

Figure 20 Fracture surfaces of trapezoid specimen and field-failed pipe [22]. The crack propagation direction is from top to bottom.

can also be noted that the trapezoid has a flatter fracture surface than the block. This difference indicates that the C–R crack plane orientation produces a more brittle failure than does the L–R crack plane orientation.

These conclusions are confirmed by comparing the side views of these three fractured specimens (Fig. 19). The arc specimen contains very large side crazes. The block specimen has thin singular side crazes, and with the exception of the initiation and final ligament regions, the trapezoid specimen is void of side crazes. Again, this shows that by preventing specimen rotation and using a C–R oriented crack, a very brittle fatigue failure can be created. Although the same crack propagation mechanism exists in each of these specimens, the adjustment of several variables has extended the region of brittle crack propagation across the entire specimen width, and the amount of damage (crazing) accompanying fracture has been significantly reduced.

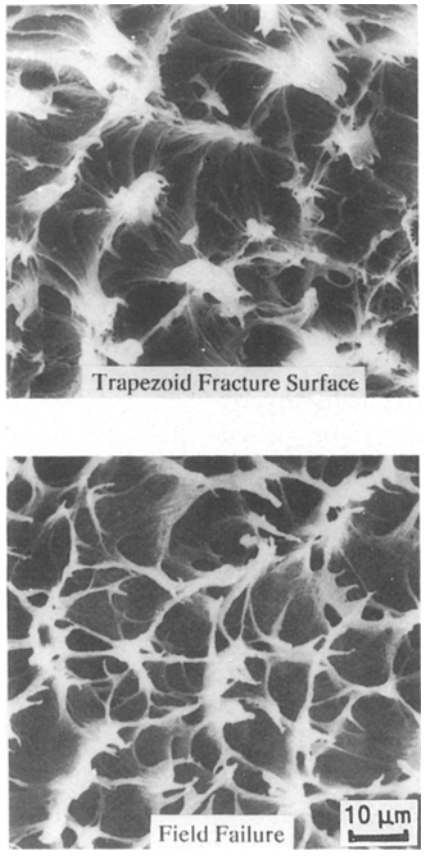

Figure 21 Microscopic comparison of trapezoid and field-failed [22] fracture surfaces.

3.2.3. Comparison with field failure

Since the objective of creating a more brittle failure was to mimic field failure, we will now compare the most brittle of the geometries – the trapezoid – with a field-failed specimen [22]. Fig. 20 shows that both the trapezoid and field failure have very similar macroscopically flat fracture surfaces, marked by several river lines. The similarity of these two specimens is striking, especially considering that the crack in the field-failed

pipe may have propagated for several years, whereas the trapezoid failure was created in three days. On a microscopic level, the same open fibre morphology is observed in both the field failure and the trapezoid specimen (Fig. 21). The likeness of these two surfaces is amazing, especially when one considers the difference in failure times. This comparison shows that fatigue can indeed be used as an accelerator in a test method which mimics the failure of pipes in service.

4. Conclusions

Fatigue fracture of MDPE pipe specimens occurs by a repetitive discontinuous mechanism in which the crack tip damage consists of a root craze and two smaller side crazes. The initially brittle fracture becomes progressively more ductile at longer crack lengths; the extent of damage increases with crack length. This ductility can be subdued by using a non-bending specimen with a C–R oriented notch. Such a specimen fails in three days and produces a fracture which closely resembles fractures observed in the field. A forked craze zone which consists of a main root craze and two smaller side crazes precedes the crack. These crazes are composed of yielded membranes rather than fibrils. At the crack tip a continuous membrane exists along the crack front; however, within the craze, the supporting structure is a network of randomly oriented membranes. Large-scale material deformation occurs outside the crazes and can be observed under polarized light.

Acknowledgement

The support of the Gas Research Institute under Contract 5083-260-2031 is gratefully acknowledged. The suggestions and assistance of Dr Max Klein, of GRI, are especially appreciated.

References

1. Annual Book of ASTM Standards, Vol. 8.04 (1988) p. D2837.
2. *Ibid.*, Vol. 8.04 (1988) p. D2290.
3. *Ibid.*, Vol. 8.04 (1988) p. D2412.
4. *Ibid.*, Vol. 8.02 (1988) p. D1693.
5. K. G. TOLL, E. F. PALERMO and G. T. APPELTON, in Proceedings of 10th Plastic Fuel Gas Pipe Symposium, New Orleans, October 1987 (American Gas Association, 1987) p. 142.
6. A. LUSTIGER and R. D. CORNELIUSSEN, *J. Mater. Sci.* **22** (1987) 2470.
7. H. NISHIMURA, T. SHISHIDO and M. NAKAKURA, in Proceedings of 9th Plastic Fuel Gas Pipe Symposium, New Orleans, November 1985 (American Gas Association, Arlington) p. 70.
8. A. MOET, A. CHUDNOVSKY, J. STREBEL and K. CHAOUI, in Proceedings of 11th Plastic Fuel Gas Pipe Symposium, San Francisco, October 1989 (American Gas Association, Arlington) p. 327.
9. Y. ZOUH, Y. LING, X. LU and N. BROWN, *ibid.* p. 321.
10. R. H. OLLEY, A. M. HODGE and D. C. BASSETT, *J. Polym. Sci. Polym. Phys. Edn* **17** (1979) 627.
11. H. SWEI, B. CRIST and S. H. CARR, *Polymer* in press.
12. A. LUSTIGER, R. L. MARKHAM and M. M. EPSTEIN, *J. Appl. Polym. Sci.* **26** (1981) 1049.
13. X. LU, R. QIAN and N. BROWN, *J. Mater. Sci.* **26** (1991) 881.
14. A. CHUDNOVSKY, A. MOET, R. J. BANKERT and M. T. TAKEMORI, *J. Appl Phys.* **54** (1983) 5562.
15. T. E. BRADY and G. S. Y. YEH, *J. Mater. Sci.* **8** (1973) 1083.
16. M. T. TAKEMORI and D. S. MATSUMOTO, *J. Polym. Sci., Polym. Phys. Edn.* **20** (1982) 2027.
17. M. D. SKIBO, R. W. HERTZBERG, J. A. MANSON and S. L. KIM, *J. Mater. Sci.* **12** (1977) 531.
18. B. D. LAUTERWASSER and E. J. KRAMER, *Phil. Mag. A* **39** (1979) 469.
19. C. C. CHAU and J. C. M. LI, *J. Mater. Sci.* **16** (1981) 1858.
20. H. H. KAUSCH and C. OUDET, *Makromol. Chem., Macromol. Symp.* **22** (1988) 207.
21. Annual Book of ASTM Standards, Vol. 2.02 (1988) p. E399.
22. A. LUSTIGER, M. J. CASSADY, F. S. URALIL and L. E. HULBERT, "Field Failure Reference Catalog for Polyethylene Gas Piping", 1st Edn (Gas Research Institute, Chicago, 1986) pp. 26, 29.

Received 21 November 1990
and accepted 15 January 1991